Journal of Biomedical Optics

SPIEDigitalLibrary.org/jbo

Effect of antiangiogenic therapy on luciferase activity in a cytomegalovirus- or HSP70-promoter-transfected M21 tumor model

Walter Hundt
Christian Schink
Silke Steinbach
Caitlin E. O'Connell-Rodwell
Andreas Kiessling
Damiano Librizzi
Mykhaylo Burbelko
Samira Guccione

SPIE

Effect of antiangiogenic therapy on luciferase activity in a cytomegalovirus- or HSP70-promoter-transfected M21 tumor model

Walter Hundt,[a,b*] Christian Schink,[c*] Silke Steinbach,[d*] Caitlin E. O'Connell-Rodwell,[e] Andreas Kiessling,[b] Damiano Librizzi,[f] Mykhaylo Burbelko,[b] and Samira Guccione[a]
[a]Stanford School of Medicine, Lucas MRS Research Center, Department of Radiology, Stanford, California
[b]Philipps University Marburg, Department of Radiology, Marburg, Germany
[c]Philipps University Marburg, Department of Clinical Cytobiology and Cytopathology, Marburg, Germany
[d]Philipps University Marburg, Department of Otolaryngology Head and Neck Surgery, Marburg, Germany
[e]Stanford School of Medicine, Department of Pediatrics, Microbiology & Immunology and Radiology, Stanford, California 94305
[f]Philipps University Marburg, Department of Nuclear Medicine, Marburg, Germany

Abstract. We investigated the effect of targeted gene therapy on heat shock protein 70 expression (*Hsp70*) and protein production (HSP70) in a melanoma tumor model (M21; M21-L). M21 and M21-L cells transfected with a plasmid containing the *Hsp70* (Hspa1b) or the cytomegalovirus (CMV) promoter and the luciferase reporter gene were injected into mice; the resulting tumors grew to a size of 650 mm^3. Mice (five per group) were intravenously treated with an Arg-Gly-Asp peptide-nanoparticle/Raf-1 kinase inhibitor protein complex [RGD-NP/RAF(-)] or with a nanoparticle control. Bioluminescence imaging (IVIS®, Xenogen, USA) was performed at 12, 24, 48, and 72 h after the treatment cycle. Western blot analysis of HSP70 protein was performed to monitor protein expression. The size of the treated M21 tumors remained fairly constant (647.8 ± 103.4 mm^2 at the beginning versus 704.8 ± 94.4 mm^3 at the end of the experiment). The size of the M21-L tumors increased, similar to the untreated control tumors. Bioluminescent imaging demonstrated that when transcription was controlled by the CMV promoter, luciferase activity decreased to $17.9\% \pm 4.3\%$ of baseline values in the treated M21 tumors. When transcription was controlled by the *Hsp70* promoter, the highest luciferase activity (4.5 ± 0.7-fold increase over base-line values) was seen 24 h after injection in the M21 tumors; however, no luciferase activity was seen in the M21-L tumors. In accordance with bioluminescent imaging, western blot analysis showed a peak in HSP70 production at 24 h after the injection of the RGD-NP/RAF(-) complex in the M21 tumors; however, no HSP70 protein induction was seen in the M21-L tumors. Thus, targeted antiangiogenic therapy can induce *Hsp70* expression and HSP70 protein in melanoma tumors. [DOI: 10.1117/1.JBO.17.6.065001]

Keywords: M21 and M21-L tumor cell line; targeted antiangiogenic therapy; Hsp70 expression; luciferase activity; bioluminescence imaging.

Paper 12133 received Feb. 23, 2012; revised manuscript received Apr. 23, 2012; accepted for publication Apr. 24, 2012; published online Jun. 5, 2012.

1 Introduction

Angiogenesis is a hallmark of cancer, since tumors cannot grow in size or metastasize without an adequate blood supply.[1,2] Endothelial cells within the angiogenic vessels are known to express several markers that are almost completely absent in normal blood vessels.[3,4] One such marker, $\alpha v\beta 3$ integrin, has gained increasing attention, because its expression level in tumor vasculature correlates with the grade of malignancy.[5,6]

Viral vectors,[7] liposomes,[8] and naked DNA[9] have all been used for the delivery of therapeutic genes to vascular tissue, but none of these approaches is specific for endothelial cells. Targeting integrin $\alpha v\beta 3$ by means of drugs may provide an opportunity to selectively destroy tumor vessels by drug targeting, without affecting the microvasculature of normal tissues. This integrin receptor potentiates the internalization of foot-and-mouth disease virus,[10] rotavirus,[11] and adenovirus,[12] thereby facilitating gene transfer. Integrin $\alpha v\beta 3$ has been successfully targeted in endothelial cells by means of nonviral gene delivery, using a small organic $\alpha v\beta 3$ ligand covalently coupled to a cationic polymerized lipid-based nanoparticle, along with a mutant form of the Raf-1 kinase inhibitor protein, which fails to bind ATP (ATP-Raf) and blocks Raf-1 activity in cultured endothelial cells.[13]

The mitogen-activated protein kinase (MAPK) cascade is a key intracellular signaling pathway that regulates diverse cellular functions, including cell proliferation, cell cycle, cell survival, angiogenesis, and cell migration. The cascade includes a diverse group of members, but is generally described as a linear signaling pathway, initiated by receptor tyrosine kinases at the cell surface and culminating in the regulation of gene transcription in the nucleus, directed by the extracellular signal-regulated kinase (Erk). Although conceptually linear, considerable cross-talk occurs between the Ras/Raf/MAPK/Erk kinase (MEK)/Erk MAPK pathway and other MAPK pathways, as well as many other signaling cascades. The Ras-Raf-MEK-ERK pathway was used because its disruption suppresses angiogenesis *in vivo* and because suppression of Raf-1 activity has been reported to promote apoptosis.[14,15]

*Both authors contributed equally to this paper.

Address all correspondence to: Walter Hundt, MD, Philipps University Marburg, Department of Radiology, Germany. Tel: 0049-6421-58-66231; Fax: 0049-6421-58-68959; E-mail: hundt@med.uni-marburg.de

0091-3286/2012/$25.00 © 2012 SPIE

Furthermore, heat shock proteins (HSPs) play an important role both in normal cellular homeostasis and in the stress response, including the development of thermotolerance and protection from cellular damage associated with stresses such as ischemia, cytokines, and energy depletion. One of the first discovered physiological functions associated with the stress-induced accumulation of the inducible HSP70 protein was the acquisition of thermotolerance, which is defined as the ability of a cell or organism to develop resistance to heat stress after prior sublethal heat exposure.[16] Data from subsequent studies indicated that the induction of the relevant gene, *Hsp70*, was associated with development of tolerance to a variety of stresses, including hypoxia,[17] ischemia,[18] acidosis,[19] energy depletion,[20] cytokines, such as tumor necrosis factor-α (TNF-α),[21] and ultraviolet radiation.[22] Bioluminescence imaging technology[23] presents the opportunity for spatial and temporal quantification of *Hsp70* promoter efficiency through *in vivo* imaging, yielding insights into production of the protein itself.

The purpose of this study was to evaluate the effect of targeted antiangiogenic gene therapy in an M21 tumor model as evaluated by bioluminescence imaging and western blot analysis, in order to more closely examine the *Hsp70* expression pattern and production of HSP70 protein in tumor tissue undergoing this type of therapy.

2 Experimental Procedures

All animal experiments were performed in compliance with institutional animal care committee guidelines and with the approval of the animal care committee.

2.1 *Reporter Construct*

Two different plasmids were used for this study. The first plasmid contained the constitutive cytomegalovirus (CMV) promoter, and the second plasmid, the heat- and stress-inducible *Hsp70* (*Hspa1b*) promoter. The plasmid pcDNA3.1(+) (Invitrogen, San Diego, CA), including a CMV promoter and a selectable marker (neor), was used as the backbone.

The luciferase gene was ligated into the plasmid to obtain the CMV-luc reporter construct. In order to obtain the *Hsp70*-luc plasmid, the *Hsp70A1* promoter (Fig. 1) was amplified from the mouse genomic DNA (Genbank accession number M76613) by polymerase chain reaction (PCR). The resulting 1926 base pair (bp) product, incorporating the *Hsp70A1* promoter fragment, was digested with the restriction enzymes *Kpn*I and *Nco*I. The *Hsp70A1* promoter sequence was replaced with the CMV promoter, and the whole fragment was then ligated into the luciferase reporter gene construct to yield the *Hsp70*-luc plasmid.

5′-
GGTACCAACCGCATCAAACCGAGGACCAACTGGGACACAGAGGCTTCTGCCCCA
CTCCAATCAGAGCCTTCCCAGCTCACCTGGGATCTCTACGCCTTCGATCCAGTTTG
GAAAATTTGAAGTCGCTGAGCCCCTACGAGCAGGGAGCTCCAGGAACATCCAAA
CTGAGCAGCCGGGGTCCCCCCCACCCCCCACCCCGCCCCTCCCGGCAACTTTGAG
CCTGTGCTGGGACAGAGCCTCTAGTTCCTAAATTAGTCCATGAGGTCAGAGGCAG
CACTGCCATTGTAACGCGATTGGAGAGGATCACGTCACCGGACACGCCCCCAGGC
ATCTCCCTGGGTCTCCTAAACTTGGCGGGGAGAAGTTTTAGCCCTTAAGTTTTAGC
CTTTAACCCCCATATTCAGAACTGTGCGAGTTGGCGAAACCCCACAAATCACAAC
AAACTGTACACAACACCGAGCTAGAGGTGATCTTTCTTGTCCATTCCACACAGGC
TTTAGTAATGCGTCGCCATAGCAACAGTGTCACTAGTAGCACCAGCACTTCCCCA
CACCCTCCCTCTCAGGAATCCGTACTTCTCCAGTGAACCCCAGAAACCTCTGGAG
AGTTCTGGACAAGGGCGGAACCCACAACTCCGATTACTCAAGGGAGGCGGGGAA
GCTCCACCAGACGCGAAACTGCTGGAAGATTCCTGGCCCCAAGGCCTCCTCCGGC
TCGCTGATTGGCCCAGCGGAGAGTGGGCGGGGCCGGTGAAGACTCCTTAAAGGC
GCAGGGCGGCGAGCAGGTCACCAGACGCTGACAGCTACTCAGAACCAAATCTGG
TTCCATCCAGAGACAAGCGAAGACAAGAGAAGCAGAGCGAGCGGCGCGTTCCCG
ATCCTCGGCCAGGACCAGCCTTCCCAGAGCATCCCTGCCGCGGAGCGCAACCTTC
CCAGGAGCATCCCTGCCGCGGAGCGCAACTTTCCCCGGAGCATCCGCGCCGCGGA
GCGCAGCCTTCCAGAAGCAGAGCGCGGCGC-3′

Fig. 1 Description of *Hsp70*A1 promoter sequence used in the *Hsp70-luc* reporter construct.

2.2 *Cells*

Human melanoma cells expressing integrin $\alpha v\beta 3$ (M21) or lacking this integrin (M21-L)[24] were incubated in RPMI 1640 culture medium (Gibco BRL , Life Technologies, USA) supplemented with 10% fetal bovine serum (FBS); (Gibco BRL, Life Technologies, USA) and antibiotics. The cells were cultured and transfected with the reporter construct, and resistant colonies were selected with Geneticin (500 μg/mL), (Gibco BRL, Life Technologies, USA). In order to assess whether the cells had been stably transfected with the *Hsp70*-luc plasmid, cells were exposed to heat stress (42°C for 20 min), and cell colonies with high luciferase activity were cultured further. The transfected CMV-luc cells also showed high luciferase activity.

2.3 *Tumor Implantation*

For tumor cell implantation, 12-week-old nude mice (Jackson Laboratories, USA) were anesthetized with intraperitoneal pentobarbital (58 mg/kg). An average of 2×10^5 tumor cells of each tumor cell line (M21, M21-L) in Hanks' solution were implanted subcutaneously (s.c.), under the dorsal skin of the flank, using a 27 G needle. The total volume of injection was 0.2 ml. The size of the tumors was measured twice a week to monitor the growth of the tumor. The tumors were measured with a microcaliper and values rounded to the nearest millimeter. Tumor size was determined by manually measuring two diameters [length (a), and width (b)]. Assuming the tumor was an oval body, tumor volume was calculated according to the following formula: $V = ab2\pi/6$. Approximately two weeks were required for tumors to grow to 650 mm^3 in size.

2.4 *Antiangiogenic Gene Therapy*

To form the Arg-Gly-Asp peptide (RGD)-conjugated nanoparticles (NP), particles containing 0.5% biotinylated lipid, 29.5% Gd^{3+}-chelator lipid, 10% amine-terminated lipid, and 60% filler lipid (PDA) were constructed. First, to synthesize the NPs, purified lipid components were dissolved in organic solvents ($CHCl_3$ and CH_3OH, in a ratio of 1:1). The $CHCl_3$ and CH_3OH were evaporated and dried in a rotary evaporator for 24 h. Distilled and deionized water was added to yield a heterogeneous solution of 30 mM total lipid concentration. The lipid/water mixture was then sonicated with a probe-tip sonicator for at least 1 h. Throughout sonication, the pH of the solution was maintained between 7.0 and 7.5 with 0.01N NaOH solution, and the temperature was maintained above the gel-liquid crystal phase transition point (Tm). The liposome solution was then transferred to a petri dish resting on a bed of ice, cooled to 0°C, and irradiated at 254 nm for at least 1 h with a hand-held UV lamp placed 1 cm above the petri dish, to yield NPs. The NPs were then filtered through a 0.2-mm filter and collected.

Using a Brookhaven dynamic light scattering system (BI-200SM multiangle laser light scattering system, Brookhaven Instruments Corporation, USA), the size (diameter) distribution and zeta potential of NPs were determined to be 45.3 ± 2.4 nm and $+35$ mV, respectively, as averaged for 17

cycles of NP synthesis. The resulting NPs were red (absorption maxima at 498 and 538 nm) and were stable at room temperature, even in the presence of serum. RGD-conjugated paramagnetic polymerized vesicles were formed using an avidin bridge to attach the RGD peptide, via biotin molecules, to the particle surface.[25,26] The ratio of the RGD peptide and avidin was 2.7 : 1.

A plasmid with a dominant-negative mutant form of *Raf-1* was used as the therapeutic agent. This Raf-1 mutant (ATP$^{\mu}$-Raf) fails to bind ATP, producing a dominant-negative effect. The plasmid and NPs are held together during assembly by electrostatic charges due to the cationic nature of the NPs and the negative charge of the plasmid. This targeted NP-plasmid complex [RGD-NP/RAF(-)] was systemically injected into the mice, through the tail vein,[13] for a total of seven times. The mice received these intravenous treatments at a dose of 1 mg/kg of NP and 1 μg/kg of the ATP$^{\mu}$-Raf-containing plasmid; the total volume for each injection was 200 μl. Control mice were injected only with the targeted nanoparticles, i.e., those lacking the ATP$^{\mu}$-Raf-containing plasmid.

2.5 *Experimental Groups*

Five animals were assigned to each experimental group, which were defined as follows: M21 or M21-L tumors transfected with the *Hsp70*-luc plasmid or with the CMV-luc plasmid, where the animals were given (1) no therapy, (2) antiangiogenic therapy, or (3) injection of the targeted-NPs only.

2.6 *Bioluminescence Imaging*

Bioluminescence imaging was performed with a highly sensitive, cooled CCD camera, mounted in a light-tight specimen box (IVIS®, Xenogen, USA), using protocols similar to those described previously.[27] Before imaging, animals were anesthetized in a plastic chamber filled with a 2% isoflurane/air mixture; 150 mg/ml of luciferin (potassium salt, Xenogen, USA) in normal saline was injected intraperitoneally (i.p.), at a dose of 150 mg/kg body weight, 10 min before imaging. This dose and route of administration have been shown to be optimal for studies in rodents when images were acquired between 10 and 20 min post-luciferin administration.[28]

For imaging, mice were placed onto the warmed stage inside the light-tight camera box, with continuous exposure to 1% to 2% isoflurane. The animals were imaged prior to any treatment, as well as at 12, 24, 48, and 72 h after the treatment cycle, and data were acquired for 60 s; this imaging time was shown to yield superior results. The low levels of light emitted from the bioluminescent tumors were detected by the IVIS® camera system and were then integrated, digitized, and displayed. The regions of interest (ROI) from displayed images were designated around the tumor area and were quantified as total photon counts or in photons/s, using Living Image® software (Xenogen, USA). The background bioluminescence *in vivo* was in the range of 1×10^4 photon counts or 1 to 2×10^5 photons.

2.7 *Immunoblot*

In order to correlate bioluminescence results with protein production, an HSP70 immunoblot experiment was performed. The treated tumors were harvested 12, 24, 48, and 72 h after injection of the RGD-NP/RAF(-) complex. The treated and untreated tumors were placed in lysis buffer (8 M urea/2% CHAPS with proteinase inhibitor) and were homogenized on ice. The homogenized slurry was transferred to a clean tube and centrifuged at 8670 × g for 10 min at 4°C (Eppendorf centrifuge 5801 R; Eppendorf, Germany). The supernatant was aliquoted to sterile microcentrifuge tubes and kept at −80 °C until use. Protein concentrations in the aliquots were measured using the Bio-Rad Protein Assay (Bio-Rad, USA) with bovine serum albumin as the standard. The equivalent of 100 μg of total protein of the sample was electrophoresed on 4% to 10% SDS-PAGE gels and then transferred onto nitrocellulose membranes (Bio-Rad, USA). Heat-shocked HeLa Cell Extract (LYC-HL101F, StressGen, USA) was coelectrophoresed as a positive control, and beta-actin antibody was used as a loading control (A5441, Sigma, USA). The nitrocellulose membrane was blocked overnight with 5% nonfat dry milk in TBST buffer (20 mM Tris-HCl, 150 mM NaCl, pH 7.4) containing 0.1% Tween 20 and then probed with the anti-HSP70 monoclonal antibody (alkaline phosphatase-conjugated SPA-810 AP, StressGen, USA). Immunodetection of the protein was achieved by the use of an enzymatic chemifluorescence (ECF) reagent (Amersham/Vistra, USA) according to the manufacturer's protocol and imaged on a phosphorimager (Amersham, USA).

2.8 *Histology*

At the end of the study, the animals were euthanized, and the treated tumors and untreated control tumor tissue were retrieved for histological analysis. For hematoxylin and eosin (H&E) staining, tissue samples were preserved in 10% formalin solution for 96 h. Subsequently, samples were embedded in paraffin, sectioned, and stained with H&E, and mounted on glass slides. Terminal deoxynucleotidyl transferase (TdT)-mediated dUTP nick-end labeling (TUNEL) assays were used for the detection of tumor apoptosis, using tumor total antioxidant capacity (TACs) kits (R&D Systems Inc. USA). Briefly, tumor samples were first fixed with 10% formaldehyde and the cell membranes permeabilized with Cytonin reagent. DNA strand breaks were then labeled with biotinylated nucleotides in TUNEL buffer at 37°C for 1 h. Apoptotic cells were visualized as brown precipitates generated by streptavidin-conjugated horseradish peroxidase in the presence of diaminobenzidine (DAB). Samples were then counterstained with 1% methylgreen to show viable cells.

2.9 *Statistical Analysis*

The mean bioluminescence (photon/s) and corresponding standard errors were determined for each experiment. The data from treated and control groups were also analyzed using the Mann-Whitney test. A p-value of <0.05 was considered statistically significant.

3 Results

The untreated M21 tumors increased from 690.8 ± 55.9 mm^3 to 1345.3 ± 55.6 mm^3 in size ($p < 0.0001$), while the untreated M21-L tumors increased from 701.0 ± 42.9 mm^3 to 1265.3 ± 34.6 mm^3 in size ($p < 0.0001$) during the experiment (19 days). No difference in size was found between the untreated M21 and M21-L tumors ($p = 0.212$), nor was there any difference in size between the untreated M21-L tumors transfected with the CMV-luc or *Hsp70*-luc plasmids ($p = 0.03$). Transcription

controlled by the CMV promoter luciferase activity increased significantly during this period by 2.5 ± 0.6-fold ($p < 0.001$), while that controlled by the *Hsp70* promoter increased by 2.9 ± 0.9-fold ($p < 0.001$).

The mean size of the treated M21 tumors did not increase as much as that of the untreated tumors; the former were on an average 659.8 ± 103.4 mm^3 at the start of the experiment, and reached a size of 704.8 ± 94.4 mm^3 by the end of the treatment. Although the increase in size of the treated M21 tumors was statistically not significant ($p = 0.080$), the increase in size differed significantly compared to that of the untreated control group ($p < 0.001$). No significant difference was seen in the initial size (636 ± 87.4 mm^3 versus 666.8 ± 109.4 mm^3; $p = 0.451$) and final size after treatment (697.8 ± 84.8 mm^3 versus 712.8 ± 104.4 mm^3; $p = 0.532$) of the M21 tumors transfected with the CMV-luc plasmid and those transfected with the *Hsp70*-luc plasmid.

The treated M21-L tumors showed growth behavior similar to that of the untreated M21 and M21-L tumors; their size increased from 698 ± 52.9 mm^3 to 1302.3 ± 102.6 mm^3 ($p < 0.001$).

3.1 *Bioluminescence Imaging*

In the M21 tumors, bioluminescence imaging demonstrated that when transcription was controlled by the CMV promoter, luciferase activity decreased under the antiangiogenesis therapy by $17.9 \pm 4.3\%$, compared to the initial luciferase activity (2.5×10^8 photons/s versus 4.5×10^7 photons/s; $p < 0.0001$). In the M21-L tumors, no difference was seen between the treated tumors and the untreated controls.

When transcription was controlled by the *Hsp70* promoter in the M21 tumors, the highest induction of luciferase activity was seen 24 h after the injection of the RGD-NP/RAF(-) complex (Fig. 2). The first three injections induced the luciferase activity by 4.5 ± 0.7-fold compared to baseline (3.8×10^7 photons/s versus 6.5×10^6 photons/s; $p < 0.001$). The subsequent three injections induced luciferase activity by between 1.9 ± 0.3- and 2.4 ± 0.4-fold (9.2×10^6 photons/s versus 4.3×10^6 photons/s; $p < 0.010$ between the fourth and fifth injection; 1.0×10^7 photons/s versus 4.2×10^6 photons/s; $p < 0.010$ between the fifth and sixth injection). Each therapy cycle reduced the baseline luciferase

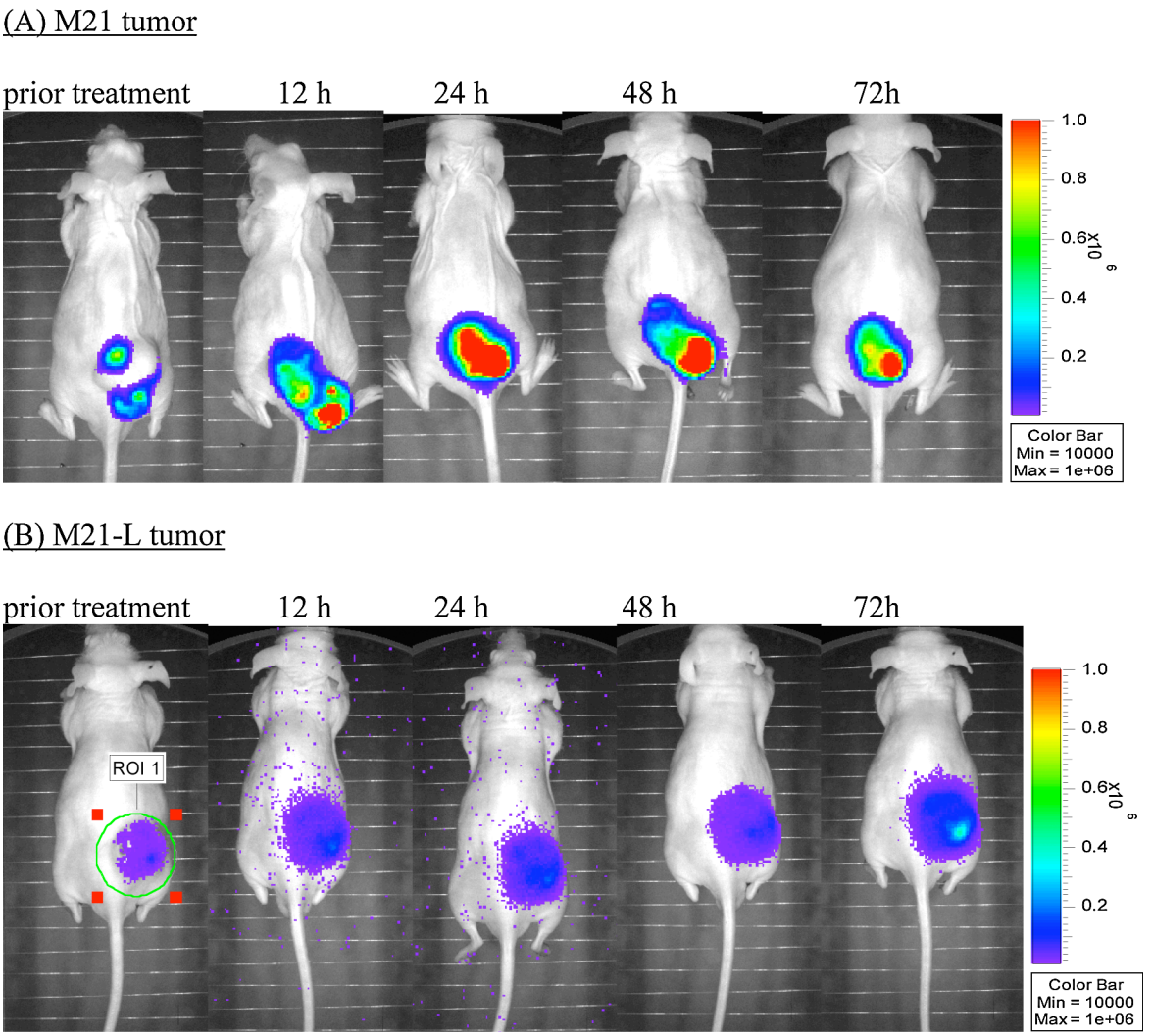

Fig. 2 Transcription controlled by the *Hsp70* promoter in M21 tumors. (a) Luciferase activity after injection of the RGD-NP/RAF(-) complex. The highest luciferase activity was seen at 24 h post injection. In the M21-L tumors (b), no increase in luciferase activity was found. Pseudocolor images representing light intensity were superimposed over the grayscale reference images, and light intensity was calculated for each animal.

activity further. After six injections, the luciferase activity of the tumors was reduced to 49.5% ± 8.1% of the initial activity (3.1×10^6 photons/s versus 6.5×10^6 photons/s; $p < 0.001$). In the M21-L tumors, no induction of luciferase activity could be detected; similar luciferase activity as in the untreated controls was observed (Fig. 3).

3.2 *Immunoblot Analysis*

Immunoblot analysis in the M21 tumors showed a correspondence between protein products and time when luciferase transcription was controlled by the *Hsp70* promoter. Protein production was 2.9-fold higher at 12 h and 4.5-fold higher at 24 h after injection of the RGD-NP/RAF(-) complex; this decreased to 2.3-fold higher after 48 h, and further to 1.2-fold higher after 72 h, than the baseline HSP70 production. The HSP70 protein production was significant higher ($p < 0.001$) at 12 and 24 h after injection of the RGD-NP/RAF(-) complex compared to the baseline HSP70 protein. In the M21-L tumors, no increase in HSP70 protein could be detected. Comparing the HSP70 protein production in the M21 to the M21-L tumors at the different time points significant differences could be found ($p < 0.01$) (Fig. 4).

3.3 *Histology*

With H&E staining, the M21 tumor tissue appeared to be dense. The tumor tissue was infiltrated with fibrous septa, and no significant areas of tumor necrosis could be found. However, after antiangiogenic therapy, significant tissue changes were found. This tissue showed irregular necrotic areas characterized by condensation and pyknosis of nuclear chromatin and shrinkage and hypereosinophilia of cell cytoplasm. The tumor tissue structure was less dense, and dilated tumor vessels could be found.

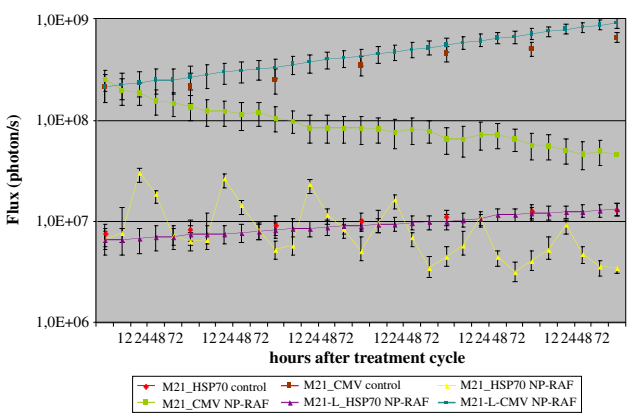

Fig. 3 Transcription controlled by the CMV and *Hsp70* promoters in the M21 and the M21-L tumors. Luciferase activity is shown for the presence and absence of antiangiogenic treatment. In the M21-*Hsp70-luc* and M21-CMV-luc control tumors, a continuous increase in luciferase activity was observed over time. In the M21-L-*Hsp70*-luc and M21-L-CMV-luc tumors treated with the RGD-NP/RAF(-) complex, no therapeutic effect was seen; rather, a continuous increase in tumor size and increase in luciferase activity was observed. In contrast, in the M21-CMV-luc transfected tumors, a continuous decrease in luciferase activity was observed in tumors treated with the RGD-NP/RAF(-) complex. In the M21-*Hsp70*-luc-transfected tumors, an increase in luciferase activity was observed 24 h after injection of this antiangiogenic therapeutic agent.

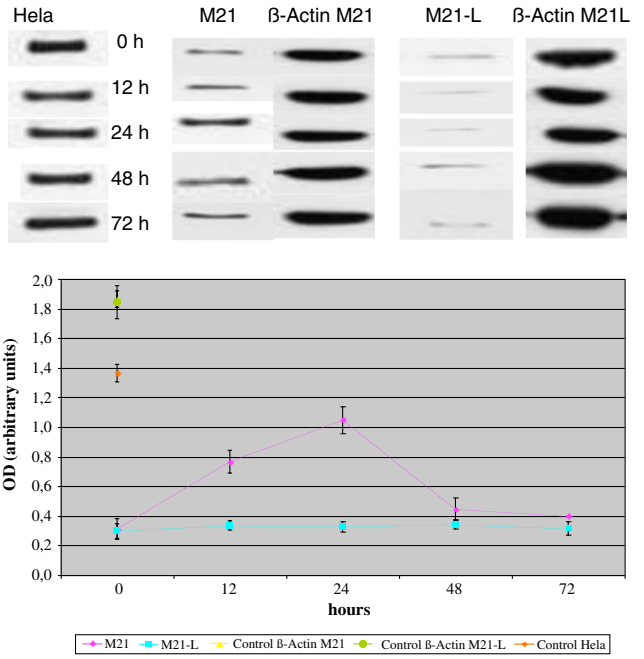

Fig. 4 Immunoblot analysis of the HSP70 protein in M21 tumors after injection of the RGD-NP/RAF(-) complex. β-Actin was used as the loading control, and heat-shocked HeLa cell extract was used as the positive control for the HSP70 protein. The optical density of the β-actin loading control, and the HSP70 protein in the heat-shocked HeLa cell extract, as well as in the M21 and M21-L tumors after injection of the RGD-NP/RAF(-) complex, were monitored by phosphoimaging. The highest HSP70 production was seen 24 h after the injection of the RGD-NP/RAF(-) complex in the M21 tumors. In the M21-L tumors, no change in HSP70 production was observed.

Moreover, TUNEL staining indicated a number of cells with markedly increased positive staining, as compared with the untreated tumors. Several apoptotic cells were observed among the remaining viable cells (Fig. 5).

4 Discussion

Angiogenesis is required for tumor progression. However, antiangiogenic agents have infrequently been tested in patients with advanced melanoma. Experience with most other cancers suggests that single-agent application of angiogenic inhibitors is unlikely to have substantial clinical antitumor activity in melanoma.

The integrin $\alpha v\beta 3$ can function as a receptor for vitronectin, and it appears to play a critical role in melanoma growth and in further metastasis.[29] This integrin is specific for tumor-associated vasculature and is required for melanoma cell survival. Moreover, $\alpha v\beta 3$-blockade has produced antitumor effects in preclinical models.[30] In the study of Hood and Cheresh,[13] it was demonstrated that $\alpha v\beta 3$-targeted delivery of ATP-Raf to blood vessels caused tumor regression because of the ability of this agent to promote apoptosis of the angiogenic endothelium.

In the present study, we combined this type of antiangiogenic therapy with bioluminescence imaging and confirmed our results by western blot analysis, as well as a histological analysis, of the tumor tissue. Bioluminescence imaging is a broadly applicable technology for assessing biological processes *in vivo*. The opportunity for spatial and temporal quantification of the CMV and *Hsp70* promoter efficiency has become possible

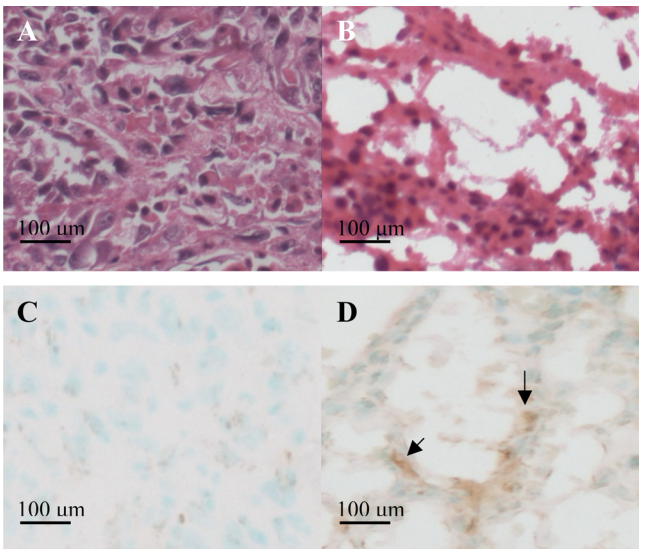

Fig. 5 Hematoxylin and eosin (H&E) staining and TUNEL staining. In the untreated M21 tumors (a), regular cells and stroma were observed by H&E staining, while in the treated tumors M21 (b), the tissue showed irregular necrotic areas characterized by condensation and pyknosis of nuclear chromatin, as well as shrinkage and hypereosinophilia of the cellular cytoplasm. TUNEL staining showed a few apoptotic cells in the untreated M21 tumors (c), while in the treated tumors (d), several apoptotic cells (arrow) were observed between the necrotic tissue and the few viable cells.

using this technology.[30] As luciferase activity can be measured in living cells[31] and tissues[32,33] and can provide a read-out of increases and decreases in transcription, it is an ideal real-time transcriptional reporter for indicating levels of *Hsp70* transcription and for providing *in vivo* information on tissue viability.[33]

In the present study, we did not see a regression in the size of the treated tumors. The tumor size in our study was approximately two times greater than that in the study by Hood and Cheresh.[13] However, over time, we did observe a significant reduction in the luciferase activity in the CMV-luc transfected M21 cell line, indicating a decrease in viable tumor cells.[33] The constant size of the tumor and the absence of tumor regression are therefore not signs of treatment failure. In targeted tumor therapy, such as with the use of angiogenesis inhibitors and anti-vascular therapies, necrosis and cavitation—without a change in size—are frequently observed. For example, single-agent treatment with sorafenib[34] and bevacizumab[35] in metastatic renal cell cancer failed to achieve significant objective response rates according to the RECIST criteria but did result in a significant increase in progression-free survival (PFS), demonstrating its clinical efficacy.

In the untreated control group, a progressive growth of the tumors and a progressive increase in luciferase activity were observed. Hood and Cheresh showed that a therapeutic effect of $\alpha v\beta 3$-targeted delivery of ATP-Raf could be achieved with several components contributing to its pronounced antitumor activity.[13] First, the NPs have multivalent targeting to integrin, enabling selective delivery of genes to angiogenic blood vessels. Second, the mutant *Raf-1* gene, when delivered to these tissues, influences the signaling cascades of two prominent angiogenic growth factors, bFGF and VEGF.[13] The robust proapoptotic activity of this gene is consistent with previous studies that have indicated a role for *Raf-1* in promoting cell survival.[36]

In the present study, we have observed the same effect of this antiangiogenic therapy, as in the Hood and Cheresh study, which demonstrated histologically that 24 h after RGD-NP/RAF (-) injection, TUNEL-positive cells were detected only among those vessels that had been transduced. The authors showed that $\alpha v\beta 3$-targeted delivery of ATP$^{\mu}$-Raf to blood vessels caused tumor regression because of its ability to promote apoptosis of the angiogenic endothelium. In our study, we applied the RGD-NP/RAF(-) complex seven times and found significant changes in the relevant tissue. The tissue showed irregular necrotic areas characterized by condensation and pyknosis of nuclear chromatin and shrinkage and hypereosinophilia of the cell cytoplasm. The tumor tissue structure was less dense, and dilated tumor vessels could be observed. While TUNEL staining of untreated tumors showed only a few apoptotic cells in the treated tumors, several apoptotic cells were observed between the necrotic tissue and the few remaining viable cells. The highest luciferase activity was seen at 24 h after injection of the RGD-NP/RAF(-) complex, correlating positively with the highest HSP70 production, as confirmed by western blot analysis. The high luciferase activity is an indirect parameter of the induction of HSPs itself, which was confirmed by western blot analysis. The goal of HSP70 protein induction is the development of tolerance as a reaction of the cells to a variety of stresses due to the antiangiogenic therapy, including hypoxia,[17] ischemia,[18] acidosis,[19] and energy depletion.[20] Thus, our results are in accordance with those of Hood and Cheresh,[13] who found that maximal luciferase activity was detected in the tumors 24 h after injection of $\alpha v\beta 3$-NP coupled to 25 μg of luciferase. In their experiment, only minimal luciferase was detected in the lungs and heart, and no detectable expression was found in the liver, brain, kidney, skeletal muscle, spleen, and bladder. In our study, we observed that the luciferase activity decreased with each treatment cycle—indicating the decrease in viable tissue—independent of whether transcription was controlled by the CMV or the *Hsp70* promoter.

Such an experimental approach combines the therapeutic effect of antiangiogenic therapy with *in vivo* imaging of gene expression and tissue changes. It enables the study of specific genes under the effect of the therapy, thus providing precise information on therapeutic efficacy.

Acknowledgments

We thank Susan J. Knox (Stanford University, Radiation Oncology, Stanford, CA) for providing the human M21 melanoma cells for this study.

References

1. D. W. J. van der Schaft et al., Tumour vasculature targeting, in *Drug Targeting: Organ-Specific Strategies*, G. Molema and D. K. F. Meijer, Eds., pp. 233–254, Wiley-VCH, Weinheim, Germany (2001).
2. D. Fukumura et al., "Tumor microvasculature and microenvironment: novel insights through intravital imaging in pre-clinical models," *Microcirculation* **17**(3), 206–225 (2010).
3. M. Friedlander et al., "Definition of two angiogenic pathways by distinct av integrins," *Science* **270**(5241), 1500–1502 (1995).
4. H. P. Hammes et al., "Subcutaneous injection of a cyclic peptide antagonist of vitronectin receptor-type integrins inhibits retinal neovascularization," *Nat. Med.* **2**(5), 529–533 (1996).
5. A. Erdreich-Epstein et al., "Integrins $av\beta 3$ and $av\beta 5$ are expressed by endothelium of high-risk neuroblastoma and their inhibition is associated with increased endogenous ceramide," *Cancer Res.* **60**(3), 712–721 (2000).

6. C. I. Baeten et al., "Prognostic role of vasculogenic mimicry in colorectal cancer," *Dis. Colon Rectum* **52**(12), 2028–2035 (2009).
7. P. Blezinger et al., "Systemic inhibition of tumor growth and tumor metastases by intramuscular administration of the endostatin gene," *Nat. Biotechnol.* **17**(4), 343–348 (1999).
8. Y. Wang and D. Becker, "Antisense targeting of basic fibroblast growth factor and fibroblast growth factor receptor-1 in human melanomas blocks intratumoral angiogenesis and tumor growth," *Nat. Med.* **3**(8), 887–893 (1997).
9. S. Takeshita et al., "Gene transfer of naked DNA encoding for three isoforms of vascular endothelial growth factor stimulates collateral development in vivo," *Lab. Invest.* **75**(4), 487–501 (1996).
10. A. Berinstein et al., "Antibodies to the vitronectin receptor (integrin alpha V beta 3) inhibit binding and infection of foot-and-mouth disease virus to cultured cells," *J. Virol.* **69**(4), 2664–2666 (1995).
11. C. A. Guerrero et al., "Integrin alpha(v)beta(3) mediates rotavirus cell entry," *Proc. Natl. Acad. Sci. USA* **97**(26), 14644–14649 (2000).
12. T. J. Wickham et al., "Integrins alpha v beta 3 and alpha v beta 5 promote adenovirus internalization but not virus attachment," *Cell* **73**(2), 309–319 (1993).
13. J. Hood et al., "Tumor regression by targeted gene delivery to the neovasculature," *Science* **296**(5577), 2404–2407 (2002).
14. N. A. Mayr et al., "Tumor perfusion studies using fast magnetic resonance imaging technique in advanced cervical cancer: a new noninvasive predictive assay," *Int. J. Radiat. Oncol. Biol. Phys.* **36**(3), 623–633 (1996).
15. H. Hawighorst et al., "Angiogenesis of uterine cervical carcinoma: characterization by pharmacokinetic magnetic resonance parameters and histological microvessel density with correlation to lymphatic involvement," *Cancer Res.* **57**(21), 4777–4786 (1997).
16. J. Landry and P. Chretien, "Relationship between hyperthermia-induced heat-shock proteins and thermotolerance in Morris hepatoma cells," *Can. J. Biochem. Cell. Biol.* **61**(6), 428–437 (1983).
17. G. M. Hahn and G. C. Li, "Thermotolerance and heat shock proteins in mammalian cells," *Radiat. Res.* **92**(3), 452–457 (1982).
18. M. S. Marber et al., "Overexpression of the rat inducible 70-kDa heat stress protein in a transgenic mouse increases the resistance of the heart to ischemic injury," *J. Clin. Invest.* **95**(4), 1446–1456 (1995).
19. M. J. Oglesbee et al., "Diabetic ketoacidosis increases extracellular levels of the major inducible 70-kDa heat shock protein," *Clin. Biochem.* **38**(10), 900–904 (2005).
20. J. L. Wang, D. S. Ke, and M. T. Lin, "Heat shock pretreatment may protect against heatstroke-induced circulatory shock and cerebral ischemia by reducing oxidative stress and energy depletion," *Shock* **23**(2), 161–167 (2005).
21. O. Partida-Rodríguez et al., "Polymorphisms in TNF and HSP-70 show a significant association with gastric cancer and duodenal ulcer," *Int. J. Cancer* **126**(8), 1861–1868 (2010).
22. F. de la Coba et al., "Prevention of the ultraviolet effects on clinical and histopathological changes, as well as the heat shock protein-70 expression in mouse skin by topical application of algal UV-absorbing compounds," *J. Dermatol. Sci.* **55**(3), 161–169 (2009).
23. C. H. Contag and M. H. Bachmann, "Advances in in vivo bioluminescence imaging of gene expression," *Annu. Rev. Biomed. Eng.* **4**, 235–260 (2002).
24. B. Felding-Habermann et al., "Involvement of integrin alpha V gene expression in human melanom tumorigenicity," *J. Clin. Investig.* **89**(6), 2018–2022 (1992).
25. R. W. Storrs et al., "Paramagnetic polymerized liposomes as new recirculating MR contrast agents," *J. Magn. Reson. Imag.* **5**(6), 719–724 (1995).
26. D. A. Sipkins et al., "Detection of tumor angiogenesis in vivo by alphaVbeta3-targeted magnetic resonance imaging," *Nat. Med.* **4**(5), 623–626 (1998).
27. A. Rehemtulla et al., "Rapid and quantitative assessment of cancer treatment response using in vivo bioluminescence imaging," *Neoplasia* **2**(6), 491–495 (2000).
28. C. H. Contag et al., "Visualizing gene expression in living mammals using a bioluminescent reporter," *Photochem. Photobiol.* **66**(4), 523–531 (1997).
29. J. C. Gutheil et al., "Targeted antiangiogenic therapy for cancer using Vitaxin: a humanized monoclonal antibody to the integrin alphavbeta3," *Clin. Cancer Res.* **6**(8), 3056–3061 (2000).
30. J. A. Prescher and C. H. Contag, "Guided by the light: visualizing biomolecular processes in living animals with bioluminescence," *Curr. Opin. Chem. Biol.* **14**(1), 80–89 (2010).
31. K. Wilson et al., "In vitro and in vivo bioluminescence reporter gene imaging of human embryonic stem cells," *J. Vis. Exp.* **2**(14), 740 (2008).
32. J. T. Wessels et al., "In vivo imaging in experimental preclinical tumor research—a review," *Cytometry* **71**(8), 542–549 (2007).
33. J. Sjollema et al., "The potential for bio-optical imaging of biomaterial-associated infection in vivo," *Biomaterials* **31**(8), 1984–1995 (2010).
34. B. Escudier et al., "Sorafenib in advanced clear-cell renal cell carcinoma," *N. Engl. J. Med.* **356**(2), 125–134 (2007).
35. J. C. Yang et al., "A randomized trial of bevacizumab, an anti-vascular endothelial growth factor antibody, for metastatic renal cancer," *N. Engl. J. Med.* **349**, 427–434 (2003).
36. M. Hüser et al., "MEK kinase activity is not necessary for Raf-1 function," *EMBO J.* **20**(8), 1940–1951 (2001).